THE JOURNAL OF PHYSICAL CHEMISTRY A

Article

pubs.acs.org/JPCA

Open Access on 07/18/2015

EPR Line Shifts and Line Shape Changes Due to Heisenberg Spin Exchange and Dipole−Dipole Interactions of Nitroxide Free Radicals in Liquids: 9. An Alternative Method to Separate the Effects of the Two Interactions Employing ^{15}N and ^{14}N

Barney L. Bales,* Michelle Meyer, and Miroslav Peric

Department of Physics and Astronomy and The Center for Supramolecular Studies California State University at Northridge Northridge, California 91330, United States

Supporting Information

ABSTRACT: A method to separate the effects of Heisenberg spin exchange (HSE) and dipole−dipole (DD) interactions on EPR spectra of nitroxide spin probes in solution by employing ^{15}N and ^{14}N nitroxide spin probes in parallel experiments is developed theoretically and tested experimentally. Comprehensive EPR measurements are reported of 4-oxo-2,2,6,6-tetramethylpiperidine-d_{16};1-^{15}N-1-oxyl (perdeuterated ^{15}N Tempone; 15pDT), in 70 wt % aqueous glycerol as functions of concentration and temperature. The method, termed the relative broadening constant method (RBCM), is demonstrated by using the present results together with those in the literature that employed perdeuterated ^{14}N Tempone (14pDT) under identical conditions. In principle, the separation of DD and HSE is dependent on the model of diffusion and molecular-kinetic parameters; however, within present day experimental uncertainties, the RBCM method turns out to be insensitive to the model. The earlier methods to separate DD and HSE by measuring the dispersion component introduced by the two interactions shows general agreement with the RBCM; however, there are discrepancies larger than estimated uncertainties due to random errors. Thus, further support is found for Salikhov's recent theory of the effects of DD and HSE on EPR spectra (*Appl. Magn. Reson.* **2010**, *38*, 237); however, detailed confirmation is still lacking. The RBCM affords a possible approach to separate HSE and DD in spectra complicated by slow motion and/or overlap with other resonance lines, allowing the method to be used in situations more complicated than low-viscosity simple liquids.

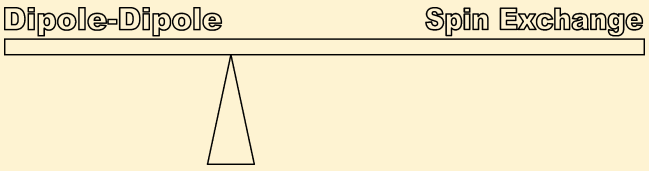

INTRODUCTION

This work adds one more tool to separate the effects of dipole−dipole interactions (DD) and Heisenberg spin exchange (HSE) on EPR spectra of dilute solutions of nitroxide free radicals (nitroxides) in low-viscosity liquids. Frequently used abbreviations and acronyms are listed in Table 1. We briefly summarize the progress to date in earlier papers in this series and refer the reader to those papers for detailed discussion. Part 1[1] demonstrated that HSE introduces a dispersion component into the spectrum from which the rate constant of HSE, K_{HSE}, may be deduced with a precision rivaling that of line broadening. In addition, Part 1[1] showed that line shifts could also be used to estimate K_{HSE}. In Part 1,[1] Fremy's salt was measured in water at 343 K where undoubtedly DD contributed negligibly to the spectrum. Parts 2,[2] 3,[3] and 4[4] continued investigations in solvents of low viscosity and at high temperatures in order to avoid DD and dealt with large values of K_{HSE}, inhomogeneous broadening, and five lines rather than the usual three. In Part 2,[2] the line shifts were found not to conform with early theoretical predictions;[5] thus, they could not be used to deduce K_{HSE}. We incorrectly speculated that the discrepancy was due to inhomogeneous broadening, B_{inhom}, caused by unresolved proton or deuteron hyperfine interactions and magnetic field modulation.[6] Part 3[3] advanced a more plausible proposal, attributing the line-shift discrepancy to HSE due to re-encounters of the same pair while residing in a cage as proposed by Salikhov.[7] Part 4[4] presented further evidence that Salikhov's re-encounter mechanism was correct, and Part 5[8] exploited the mechanism to study re-encounter collisions in a series of alkanes. Finally, in Part 6,[9] we purposely studied a viscous liquid, 70 wt % glycerol in water (70%AG), in order to address the separation of DD and HSE.

Table 1. Abbreviations and Acronyms

DD	dipole−dipole interactions
HSE	Heisenberg spin exchange
nitroxides	nitroxide free radicals
SE	Stokes−Einstein equation
instrumental dispersion	in phase magnetization, commonly due to an improperly balanced microwave bridge
B_{inhom}	inhomogeneous broadening caused by unresolved proton or deuteron hyperfine interactions and magnetic field modulation
FIT or FITTING	linear or nonlinear least-squares fit, noun or verb
70%AG	70 wt % glycerol in water
HVL	high-viscosity limit to evaluate DD contributions
LVL	low-viscosity limit to evaluate DD contributions

Received: May 30, 2014
Revised: July 16, 2014
Published: July 18, 2014

   dx.doi.org/10.1021/jp505346g | *J. Phys. Chem. A* 2014, 118, 6154−6162

The premise in Part 6[9] was that the effects of DD could be sufficiently described using motional narrowing theory; thus, DD was assumed not to contribute to dispersion components or line shifts. Therefore, the dispersion component was used to estimate the effects of HSE and the remainder due to DD. This approach gave reasonable results, with the effects being dominated by HSE at high temperatures and by DD at low temperatures. Two problems arose: (1) negative values of the dispersion were encountered at low temperatures and (2) the variation of the dispersion with the line broadening, predicted to be linear, were found to be nonlinear. A reviewer of Part 6[9] called our attention to ref 10 that showed that DD produces negative values of the dispersion. Thus, Part 6[9] supported the need to include a detailed account for the effects of DD and we encouraged the development of the theory in ref 10 for nitroxides. The following year, Salikhov did just that[11] and we responded with Part 8[12] using a high-viscosity alkane, squalane, employing many more low-concentration samples than in Part 6.[9] Thus, a negative dispersion component was explained; however, the problem of its nonlinear variation with the broadening persisted. We had speculated in Part 6[9] that the DD contribution to the dispersion persisted only up to a critical concentration; above that, it did not contribute further and Part 8 seemed to support this unlikely notion because clear linear segments below a critical concentration and other linear segments above that were observed. If we analyzed the lower segments including DD and upper without DD, we got the same results. Nevertheless, that DD should stop contributing above a critical concentration was not explained.

Salikhov[11] remarked that "EPR investigations of ^{14}N and ^{15}N nitroxide radicals can give complementary results." The story would be better if we had then carried out investigations using ^{15}N in 70%AG to complement those in Part 6;[9] however, we had already done these studies in parallel with those using ^{14}N in Part 6 with the vague notion that they could be useful. They have indeed turned out to be useful.

THEORY

Effects of DD and HSE. The effects of DD and HSE on EPR spectra of ^{14}N and ^{15}N nitroxide free radicals (nitroxides) were treated by Salikhov.[11] Kinetic eqs 1 and 10 of ref 11 encompass these effects by taking into account the loss of spin coherence (W) and the transfer of spin coherence (V) due to both DD and HSE. Thus,

$$ {}^{A}W = {}^{A}W_{\mathrm{HSE}} + {}^{A}W_{\mathrm{DD}} \tag{1} $$

and

$$ {}^{A}V = {}^{A}V_{\mathrm{HSE}} + {}^{A}V_{\mathrm{DD}} \tag{2} $$

where the superscript A denotes the mass number and the subscripts, the interaction. Terms in eq 1 broaden the lines of the EPR spectrum, while those in eq 2 introduce a dispersion component and shift the resonance fields of the lines. In terms of the rate constant of HSE, K_{HSE}, which is the same for both isotopes under the same conditions,[11]

$$ {}^{A}W_{\mathrm{HSE}} = \frac{2I}{2I+1}K_{\mathrm{HSE}} \tag{3} $$

Also,

$$ {}^{A}V_{\mathrm{HSE}} = \frac{1}{2I+1}K_{\mathrm{HSE}} \tag{4} $$

where I is the ^{A}N nuclear spin quantum number.

Contributions to ${}^{A}W_{\mathrm{DD}}$ are different for like or unlike spins, eqs 79 or 89 of ref 13, respectively. For nitroxides, the fraction $2I/(2I+1)$ or $1/(2I+1)$ of the collisions are with a different spin or a like spin, respectively. We find the following:

$$ {}^{A}W_{\mathrm{DD}} = \kappa^2\left[\frac{3}{8}J^{(2)}(2\omega_0) + \frac{18I+15}{4(2I+1)}J^{(1)}(\omega_0) + \frac{10I+9}{24(2I+1)}J^{(0)}(0)\right]N_{\mathrm{A}}(10^{-3}) \tag{5} $$

with $\kappa^2 = 3\gamma^4\hbar^2/4$ for electron spins, where γ is the gyromagnetic ratio of the electron, $J^{(n)}(\omega)$ are the spectral densities of the correlation functions for DD, ω is the microwave frequency, and N_{A} is Avogadro's number. Equation 5 agrees with the corresponding equations on pp 239 and 240 of ref 11. The spectral densities are usually given in concentration units cm^{-3},[11,13] and the factor $N_{\mathrm{A}}(10^{-3})$ changes the units to molarity.

From p 240 of ref 11,

$$ {}^{A}V_{\mathrm{DD}} = -\frac{1}{(2I+1)}\kappa^2\left[\frac{3}{2}J^{(1)}(\omega_0) + \frac{1}{6}J^{(0)}(0)\right]N_{\mathrm{A}}(10^{-3}) \tag{6} $$

Relationships between Rate Constants and Measurable Parameters. For definiteness, we restrict our development to first-derivative EPR spectra with the detection phase adjusted so that the doubly integrated intensity is positive. For ^{14}N, $M_j = +1, 0, -1$, the ^{14}N nuclear quantum numbers, label the low-, middle-, and high-field lines, respectively. For convenience, for ^{15}N, we assign $M_j = +1$ and -1 as the labels of the low- and high-field lines, respectively. Thus, for ^{15}N, M_j is equal to minus twice the corresponding nuclear quantum number.

Previous papers in this series[1−4,9] have detailed nonlinear least-squares fitting of the EPR spectra and how the following quantities are obtained: (1) the peak-to-peak line width of the Lorentzian component, $\Delta H^{L}_{\mathrm{pp}}(M_j)$, of each of the resonance lines, (2) the ratios $M_j(V_{\mathrm{disp}}/V_{\mathrm{pp}})_{M_j}$ for each line, where V_{disp} is the extremum value of the dispersion component and V_{pp} is the peak-to-peak height of the absorption component, and (3) the resonance fields of the lines, H_{M_I}. Observed values of $M_j(V_{\mathrm{disp}}/V_{\mathrm{pp}})_{M_j}$ are corrected for instrumental dispersion and for a small nonlinearity as detailed in the Supporting Information. These corrected values, calculated with eqs S4 and S7, are denoted $\pm\,{}^{A}(V_{\mathrm{disp}}/V_{\mathrm{pp}})^{\#}_{\pm}$. Values of $\pm\,{}^{A}(V_{\mathrm{disp}}/V_{\mathrm{pp}})^{\#}_{\pm}$ are positive if HSE dominates and negative if DD dominates. In other words, the extremum of the dispersion component of the low-field line is positive and that of the high-field line is negative if HSE dominates; the opposite holds if DD dominates.

The line broadening due to DD and HSE for each line is computed from the following:

$$ B_{M_j} = \Delta H^{L}_{\mathrm{pp}}(c)_{M_j} - \Delta H^{L}_{\mathrm{pp}}(0)_{M_j} \tag{7} $$

where c is the molar concentration. As discussed previously (Figure 7 of ref 2), as K_{HSE} increases, the broadening of the outer lines becomes slightly larger than that of the central line in ^{14}N spectra and the average over the three lines must be used. This effect does not arise in ^{15}N spectra. For convenience, in the rest of this paper, the symbol ${}^{A}B$ is the average broadening; the standard deviation will be used, in part, to estimate the error.

For either isotope, the relationship between line broadening and ${}^{A}W$ is as follows:

$$ {}^{A}B = {}^{A}B_{\mathrm{HSE}} + {}^{A}B_{\mathrm{DD}} = \frac{2}{\sqrt{3}\gamma}\cdot{}^{A}W\cdot c \tag{8} $$

dx.doi.org/10.1021/jp505346g | J. Phys. Chem. A 2014, 118, 6154−6162

Thus,

$$ {}^{A}B_{\mathrm{HSE}} = \frac{2}{\sqrt{3}\gamma}{}^{A}W_{\mathrm{HSE}}\cdot c = \frac{2}{\sqrt{3}\gamma}\frac{2I}{(2I+1)}K_{\mathrm{HSE}}\cdot c \tag{9} $$

and

$$ {}^{A}B_{\mathrm{DD}} = \frac{2}{\sqrt{3}\gamma}{}^{A}W_{\mathrm{DD}}\cdot c \tag{10} $$

The relationship between $\pm\,{}^{A}(V_{\mathrm{disp}}/V_{\mathrm{pp}})^{\#}_{\pm}$ and ${}^{A}V$ follows from the development of eq 20 of ref 1,

$$ \pm\left(\frac{V_{\mathrm{disp}}^{\mathrm{HSE}}}{V_{\mathrm{pp}}}\right)^{\#}_{\pm} = \frac{4}{3\sqrt{3}\gamma^{A}A_0}K_{\mathrm{HSE}}\cdot c \tag{11} $$

for either isotope. Thus,

$$ \pm\left(\frac{V_{\mathrm{disp}}^{\mathrm{HSE}}}{V_{\mathrm{pp}}}\right)^{\#}_{\pm} = \frac{4}{3\sqrt{3}\gamma^{A}A_0}(2I+1)\cdot{}^{A}W_{\mathrm{HSE}}\cdot c \tag{12} $$

where ${}^{A}A_0$ (${}^{15}A_0$ or ${}^{14}A_0$) are the hyperfine spacings in the absence of DD and HSE; ${}^{14}A_0 = \lim_{c\to 0}(H_{-1} - H_{+1})/2$ or ${}^{15}A_0 = \lim_{c\to 0}(H_{-1} - H_{+1})$. From the known nuclear magnetic dipole moments of the two isotopes, ${}^{15}A_0 = 1.403\,{}^{14}A_0$. The rate constants ${}^{A}V_{\mathrm{HSE}}$ and ${}^{A}V_{\mathrm{DD}}$ enter into the kinetic equations symmetrically, so the same forms as eqs 12 also hold for $\pm\,{}^{A}(V_{\mathrm{disp}}^{\mathrm{DD}}/V_{\mathrm{pp}})_{\pm}$; thus, adding the HSE and DD contributions, $\pm\,{}^{A}(V_{\mathrm{disp}}/V_{\mathrm{pp}})_{\pm} = \pm\,{}^{A}(V_{\mathrm{disp}}^{\mathrm{DD}}/V_{\mathrm{pp}})_{\pm} \pm {}^{A}(V_{\mathrm{disp}}^{\mathrm{HSE}}/V_{\mathrm{pp}})_{\pm}$, we get

$$ \pm\left(\frac{V_{\mathrm{disp}}}{V_{\mathrm{pp}}}\right)^{\#}_{\pm} = \frac{4}{3\sqrt{3}\gamma^{A}A_0}(2I+1)\cdot{}^{A}V\cdot c \tag{13} $$

It is convenient to define the ratios ${}^{A}b \equiv {}^{A}V_{\mathrm{DD}}/{}^{A}W_{\mathrm{DD}}$, which are given in Table 2.

Separating HSE and DD Using the Dispersion Component. A useful measure of the relative importance of DD and HSE is the fractional broadening by HSE, denoted by ${}^{A}\Omega$ as follows:

$$ {}^{A}\Omega \equiv {}^{A}B_{\mathrm{HSE}}/{}^{A}B = {}^{A}B_{\mathrm{HSE}}/({}^{A}B_{\mathrm{DD}} + {}^{A}B_{\mathrm{HSE}}) \tag{14} $$

In terms of the rate constants, we have

$$ {}^{A}\Omega = \frac{{}^{A}W_{\mathrm{HSE}}}{{}^{A}W_{\mathrm{HSE}} + {}^{A}W_{\mathrm{DD}}} = \frac{K_{\mathrm{HSE}}}{K_{\mathrm{HSE}} + (2I+1)\,{}^{A}W_{\mathrm{DD}}/2I} \tag{15} $$

By eliminating K_{HSE} from eq 15, which is the same for both isotopes, we find the following identities:

$$ {}^{15}\Omega = \frac{{}^{14}\Omega}{{}^{14}\Omega(1 - 2^{14}b/{}^{15}b) + 2^{14}b/{}^{15}b} \tag{16a} $$

$$ {}^{14}\Omega = \frac{{}^{15}\Omega}{{}^{15}\Omega(1 - {}^{15}b/2^{14}b) + {}^{15}b/2^{14}b} \tag{16b} $$

Therefore, values of ${}^{A}\Omega$ determined with one isotope may be expressed in terms of the other. The HSE and DD contributions to the line broadening are given by

$$ {}^{A}B_{\mathrm{HSE}} = {}^{A}\Omega\cdot{}^{A}B \tag{17} $$

$$ {}^{A}B_{\mathrm{DD}} = (1 - {}^{A}\Omega)\cdot{}^{A}B \tag{18} $$

Expanding eq 13, utilizing eq 12 and a similar equation for $\pm\,{}^{A}(V_{\mathrm{disp}}^{\mathrm{DD}}/V_{\mathrm{pp}})_{\pm}$ employing ${}^{A}W_{\mathrm{DD}} = -{}^{A}V_{\mathrm{DD}}/{}^{A}b$, we find

$$ \pm\left(\frac{V_{\mathrm{disp}}}{V_{\mathrm{pp}}}\right)^{\#}_{\pm} = {}^{A}k\frac{{}^{A}B}{{}^{A}A_0} \tag{19} $$

where

$$ {}^{A}k = \frac{2}{3}(2I+1)\left(\left(\frac{1}{2I} + {}^{A}b\right){}^{A}\Omega - {}^{A}b\right) \tag{20} $$

We may obtain ${}^{A}k$ in terms of the rate constants by inserting eq 15 into eq 20, which yields

$$ {}^{A}k = \frac{2}{3}(2I+1)\left[\frac{K_{\mathrm{HSE}} - {}^{A}b(2I+1)\,{}^{A}W}{2IK_{\mathrm{HSE}} + (2I+1)\,{}^{A}W}\right] \tag{21} $$

or, with ${}^{A}b = -{}^{A}V_{\mathrm{DD}}/{}^{A}W_{\mathrm{DD}}$

$$ {}^{A}k = \frac{2}{3}(2I+1)\frac{K_{\mathrm{HSE}} + (2I+1)\,{}^{A}V_{\mathrm{DD}}}{2IK_{\mathrm{HSE}} + (2I+1)\,{}^{A}W_{\mathrm{DD}}} \tag{22} $$

Therefore, from slopes of the linear plots of $\pm\,{}^{A}(V_{\mathrm{disp}}/V_{\mathrm{pp}})^{\#}_{\pm}$ versus ${}^{A}B/{}^{A}A_0$, we may compute values of ${}^{A}\Omega$ using the following:

$$ {}^{A}\Omega = \frac{\left[\frac{3I}{(2I+1)}{}^{A}k + 2I\,{}^{A}b\right]}{(1 + 2I\,{}^{A}b)} \tag{23} $$

The equations in this section were reconfirmed by simulating the kinetic equations in ref 11 for both isotopes and FITTING as described recently in ref 12.

Values of ${}^{15}k$ or ${}^{14}k$ may also be found from line shifts as detailed in the Supporting Information. For ^{15}N, the two methods yield results that are within experimental uncertainty except at high temperatures. We use the values from the dispersion method because the range of permissible values of ${}^{A}B/{}^{A}A_0$ is larger than with the line shift method.

Separating HSE and DD Using the Ratio of the Broadening Constants. The RBCM. Identical experiments

Table 2. Definitions of DD Quantities and Their Values in the HVL and LVL

	high viscosity	low viscosity	% change[a]
$^{15}b = \frac{\frac{1}{2}\left[\frac{3}{2}J^{(1)}(\omega_0) + \frac{1}{6}J^{(0)}(0)\right]}{\frac{3}{8}J^{(2)}(2\omega_0) + 3J^{(1)}(\omega_0) + \frac{7}{24}J^{(0)}(0)}$	2/7	1/5	30
$^{14}b = \frac{\frac{1}{3}\left[\frac{3}{2}J^{(1)}(\omega_0) + \frac{1}{6}J^{(0)}(0)\right]}{\frac{3}{8}J^{(2)}(2\omega_0) + \frac{11}{4}J^{(1)}(\omega_0) + \frac{19}{72}J^{(0)}(0)}$	4/19	1/7	32
${}^{15}b/{}^{14}b$	19/14	7/5	−3
${}^{14}B'_{\mathrm{DD}}/{}^{15}B'_{\mathrm{DD}}$	19/21	14/15	3

[a](result at high viscosity − result at low viscosity) × 100/(result at high viscosity).

dx.doi.org/10.1021/jp505346g | J. Phys. Chem. A 2014, 118, 6154−6162

using each isotope afford another, independent, means to measure ${}^{A}\Omega$. Forming the ratio of the broadening constants noting that ${}^{A}B_{ex} = {}^{A}\Omega {}^{A}B$, using eq 9 yields the following:

$$\frac{d^{14}B/dc}{d^{15}B/dc} = \frac{{}^{15}\Omega}{{}^{14}\Omega}\frac{d^{14}B_{HSE}/dc}{d^{15}B_{HSE}/dc} = \frac{{}^{15}\Omega}{{}^{14}\Omega}\frac{4}{3} \tag{24}$$

For convenience, we use the notation $F' = dF/dc$ in the following equations but not in the figure labels.

Employing the identities, eqs 16 to eliminate ${}^{15}\Omega$ from eq 24, we arrive at the following, which complements the previous eq 23:

$${}^{14}\Omega(\mathrm{RBCM}) = \frac{\frac{3}{2}\frac{{}^{14}b}{{}^{15}b} - \frac{{}^{15}B'}{{}^{14}B'}}{\frac{3}{2}\frac{{}^{14}b}{{}^{15}b} - \frac{3}{4}} \tag{25}$$

${}^{15}\Omega(\mathrm{RBCM})$ follows from eq 16a, but it is important to note that only one independent value of ${}^{A}\Omega(\mathrm{RBCM})$ may be computed.

Dependence on the Model of Nitroxide Diffusion. In principle, the values of the parameters ${}^{14}b$ and ${}^{15}b$ depend on the details of the molecular diffusion through their dependences on $J^{(n)}(\omega)$.[11] In Table 2, these values are evaluated in the high-viscosity limit (HVL), where $J^{(2)}(2\omega_0) \to 0$ and $J^{(1)}(\omega_0) \to 0$, and low-viscosity limit (LVL), where $J^{(2)}(2\omega_0):J^{(1)}(\omega_0):J^{(0)}(0) = 4:1:6$. See after eq VIII.79 of ref 13. Observe from Table 2 that ${}^{14}b$ and ${}^{15}b$ vary at most by about 30%, while their ratio, ${}^{14}b/{}^{15}b$, by only about 3%. We demonstrated in ref 12 by using the permanent diffusion model that even with a 30% potential change in ${}^{14}b$, for typical nitroxides, the HVL limit is sufficient because at viscosities low enough for these approximations to begin to break down, HSE dominates to the extent that it is difficult to determine the effects of DD with sufficient accuracy to observe any departure from the HVL.

We note that while the simplification of using the HVL facilitates the analysis, it comes with the price of making it difficult to learn details of the diffusion mechanism from DD. A possible remedy would be to utilize a radical that severely suppresses HSE exposing the smaller DD effects.

In the HVL, eq 5 becomes the following:

$${}^{A}W_{DD} = \kappa^2\left[\frac{10I+9}{24(2I+1)}J^{(0)}(0)\right]N_A(10^{-3}) \tag{26}$$

combining eqs 5 and 10, utilizing an equation on p 252 of ref 11 for $J^{(0)}(0)$, we find that

$${}^{A}B_{DD} = \frac{2}{\sqrt{3}\gamma}\gamma^4\hbar^2\frac{(10I+9)}{(2I+1)}\frac{\pi}{75}\frac{1}{dD}N_A(10^{-3})\cdot c \tag{27}$$

where d is the distance of closest approach and D is the diffusion coefficient for one nitroxide. Using the Stokes–Einstein (SE) equation,[14] $D = kT/6\pi r\eta$, where r is the effective hydrodynamic radius and k the Boltzmann constant, assuming that the distance of closest approach is twice the hydrodynamic radius, $d = 2r$, we obtain

$${}^{A}B_{DD} = \gamma^3\hbar^2\frac{(10I+9)}{(2I+1)\sqrt{3}}\frac{2\pi^2}{25k}\frac{\eta}{T}N_A(10^{-3})\cdot c \tag{28}$$

Therefore,

$${}^{A}B'_{DD} = \frac{2\gamma^3\hbar^2\pi^2N_A(10^{-3})(10I+9)}{25(2I+1)\sqrt{3}k}\frac{\eta}{T} \tag{29}$$

Equation 29 is identical to eq 11 in ref 14.

The Stoke–Einstein form of ${}^{A}B'_{HSE}$ is the well-known[5,14]

$${}^{A}B'_{HSE} = \frac{I}{2I+1}\frac{16N_Ak(10^{-3})}{3\sqrt{3}\gamma}\frac{T}{\eta} \tag{30}$$

We thus have three independent measures of ${}^{A}\Omega$, two from the slopes of plots of $\pm\,{}^{A}(V_{disp}/V_{pp})^{\#}_{\pm}$ versus ${}^{A}B/{}^{A}A_0$, ${}^{15}k$, or ${}^{14}k$, eq 23, and another from the ratio of the broadening constants, ${}^{14}B'/{}^{15}B'$, eq 25. We evaluate the expressions in eqs 23 and 25 using the HVL as follows:

$${}^{15}\Omega({}^{15}k) = \frac{21{}^{15}k+8}{36} \tag{31a}$$

$${}^{14}\Omega({}^{14}k) = \frac{19{}^{14}k+8}{27} \tag{31b}$$

$${}^{14}\Omega(\mathrm{RBCM}) = \frac{28}{9} - \frac{76}{27}\frac{{}^{15}B'}{{}^{14}B'} \tag{31c}$$

and the identities in eqs 16 become

$${}^{15}\Omega = \frac{19{}^{14}\Omega}{28 - 9{}^{14}\Omega} \tag{32a}$$

$${}^{14}\Omega = \frac{28{}^{15}\Omega}{9{}^{15}\Omega + 19} \tag{32b}$$

Writing the separated broadening constants in eqs 17 and 18 explicitly for the HVL yields the following:

$${}^{15}B'_{HSE} = \frac{21{}^{15}k+8}{36}{}^{15}B' \tag{33a}$$

$${}^{14}B'_{HSE} = \frac{19{}^{14}k+8}{27}{}^{14}B' \tag{33b}$$

$${}^{14}B'_{HSE}(\mathrm{RBCM}) = \frac{28}{9}{}^{14}B' - \frac{76}{27}{}^{15}B' \tag{33c}$$

and

$${}^{15}B'_{DD} = \frac{28 - 21{}^{15}k}{36}{}^{15}B' \tag{34a}$$

$${}^{14}B'_{DD} = \frac{19 - 19{}^{14}k}{27}{}^{14}B' \tag{34b}$$

$${}^{14}B'_{DD}(\mathrm{RBCM}) = \frac{76}{27}{}^{15}B' - \frac{19}{9}{}^{14}B' \tag{34c}$$

Three independent values of ${}^{A}B'_{HSE}$ and of ${}^{A}B'_{DD}$ are found from eqs 33 and 34, respectively; thus the theoretical predictions that ${}^{14}B'_{HSE} = 4{}^{15}B'_{HSE}/3$ and ${}^{14}B'_{DD} = 19{}^{15}B'_{DD}/21$ may be checked from three independent measurements. Equations 31–34 are written explicitly in the LVL in the Supporting Information.

The propagated uncertainties due to random errors are amplified in the RBCM over the experimental errors in deducing ${}^{14}B'$ and ${}^{15}B$. This follows from a standard treatment[15] of the uncertainties (σ) as follows:

$${}^{14}\sigma^2_{{}^{14}B'_{HSE}} = \left(\frac{76}{27}\sigma_{{}^{15}B'}\right)^2 + \left(\frac{28}{9}\sigma_{{}^{14}B'}\right)^2 \tag{35}$$

$${}^{14}\sigma^2_{{}^{14}B'_{DD}} = \left(\frac{76}{27}\sigma_{{}^{15}B'}\right)^2 + \left(\frac{19}{9}\sigma_{{}^{14}B'}\right)^2 \tag{36}$$

dx.doi.org/10.1021/jp505346g | J. Phys. Chem. A 2014, 118, 6154–6162

Thus, uncertainties in ${}^{A}B'_{HSE}$ and of ${}^{A}B'_{DD}$ are 3−4 times larger than the uncertainties in ${}^{A}B'$. Using the dispersion methods, the propagated uncertainties are of the same order as those of the measurements.

MATERIALS AND METHODS

This work was performed at the same time as that using 14pDT in 70%AG, published in ref 9. 15pPDT (lot no. A91BP2, 99 atom % D, 99 atom % ^{15}N) was purchased from CDN Isotopes and used as received. ACS reagent glycerol (99.8%) was obtained from Sigma and used as received to prepare 70%AG with Milli-Q water. An 85 mM stock solution of 15pDT was prepared and diluted by weight to give 70, 56, 42, 21, and 0.1 mM samples. The relative concentrations are accurate to ±0.1%. Undegassed samples were sealed into 50 μL pipettes and placed into sample tubes housed in Bruker's nitrogen gas-flow temperature control dewar. The temperature, accurate to ±1 K, was measured with a thermocouple placed just above the active portion of the microwave cavity. During each spectrum, the temperature was stable to ±0.1 K. Three EPR spectra were acquired, one after the other, with a Bruker 300 ESP X-band spectrometer interfaced with Bruker's computer employing a sweep time of 41 s; time constant, 10 ms; microwave power, 5 mW; sweep width, 50.2 G; and modulation amplitude, 0.2 G. We routinely set the modulation amplitude to near the narrowest line width in a study to increase the signal-to-noise ratio of low-concentration samples, exploiting the fact[6] that field modulation does not contribute to the Lorentzian component of the line.[6] The magnetic field sweep-width of each spectrum was measured with Bruker's NMR Gaussmeter operating in the 1 mG resolution mode and was averaged over a day's run. Spectra were obtained using an automated routine raising the temperature in 5 K increments from 273 to 353 K and then decreasing the temperature between 346.5 to 276.5 K for a total of 29 temperatures remaining at each temperature 5 min before acquiring the spectra.

RESULTS

The first trace of Figure 1 shows a spectrum of 85 mM 15pDT in 70%AG at 273 K together with the residual, which is the difference in the FIT and the spectrum. The second trace shows the separated absorption and dispersion components. The residual is substantial, similar to that observed with 14pDT in the same solvent at the same temperature; Figure 3 of Part 6.[9] These residual lines are provoked by the presence of ^{13}C lines in natural abundance and are much more prominent at low values of T/η. For example, at 343 K, the residual is imperceptible; Figure 1 of Part 6.[9] In addition to the pair of ^{13}C lines about each main line, there is an apparent line midway between those lines that develops as the concentration increases. This additional line is an artifact of the FITTING and is a cause for concern because it could influence the values of the dispersion components, introducing a systematical error that is difficult to estimate. On the other hand, because the extra lines in the residual are antisymmetric and the dispersion lines are symmetric about the resonance fields, the influence could be minor. Note that because the extremum of the dispersion component is negative for the low-field line and positive for the high-field line, $\pm\,{}^{15}(V_{disp}/V_{pp})_{\pm} < 0$; i.e., DD dominates.

Values of ${}^{15}B$, as functions of c (not shown), are excellent straight lines with coefficients of correlation $r > 0.999$ similar to Figure 4 of Part 6[9] or Figure 6 of Part 8.[12] The slopes of plots of

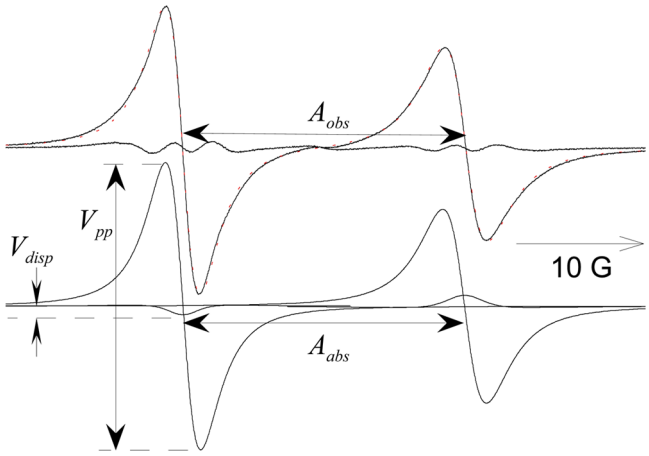

Figure 1. First trace, experimental EPR spectrum of 85 mM 15pDT in 70%AG at 273 K and the residual (the difference in the spectrum and the FIT). The residual is dominated by two ^{13}C lines for each ^{15}N line plus another line midway between each pair of ^{13}C lines that is an artifact of the FIT. The second trace shows the separated absorption and dispersion components. The extremum of the dispersion is negative for the low-field line and positive for the high-field; therefore, $\pm\,{}^{15}(V_{disp}/V_{pp})_{\pm} < 0$ showing that DD dominates. The spacing between where the experimental lines cross the baseline, A_{obs}, and between the resonance fields (where the absorption lines cross the baseline), A_{abs}, are indicated. The difference between A_{obs} and A_{abs} is imperceptible on this scale but may be measured with remarkable precision as is shown in the Supporting Information.

${}^{A}B$ vs c yield the broadening constants ${}^{14}B'$ and ${}^{15}B'$, which are shown in Figure 2a for the two isotopes; Figure 2b shows their ratios. Data for the open squares in Figure 2a were taken from Part 6.[9] The error bars are FIT errors in finding the slope of the straight lines plus the standard deviation over the two or three lines, respectively. Those in Figure 2b are the propagated errors due to finding the ratio of the two broadening constants. Thus, Figure 2b does not include any estimate of possible systematic errors in temperature or concentration between the two runs in 70%AG.

Figure 3 shows values of the normalized dispersion of the low-field line of 15pDT as functions of the normalized broadening at several representative temperatures. Figure 3 is remarkable because, unlike 14pDT in 70%AG, Figure 6b of Part 6,[9] or in squalane, Figure 8 of Part 8,[12] these data are linear even at 273 K. Thus, for the first time, there is unequivocal evidence for Salikhov's proposal[11] that DD yields negative dispersion components that are linear in the concentration (linear in ${}^{A}B/{}^{A}A_0$).

We have regularly observed that the normalized dispersion, while linear, does not extrapolate to the origin. See Figure 12 of ref 12. Recently, we found evidence that this defect is due to an inherent negative dispersion component in the absence of DD and HSE that increases in magnitude as the rotational correlation time becomes longer. See Figure 4 of ref 16 and the discussion therein. Taking ${}^{15}k(\mathrm{disp})$ to be the slope of the lines in Figure 3 is certainly reasonable, but allowing an intercept in the FIT is a source of possible systematic errors.

Values of ${}^{14}k$ were derived from the data in Part 6 from fits to eq 19. The two values from the low- and high-field lines were averaged. The errors were estimated by adding the average estimated uncertainties from the fits to one-half the difference between the results for the low- and high-field lines.

Values of ${}^{15}B'_{HSE}$ and ${}^{14}B'_{HSE}$ were computed from eqs 33a and 33b, respectively, while the uncertainties were propagated in the

dx.doi.org/10.1021/jp505346g | J. Phys. Chem. A 2014, 118, 6154−6162

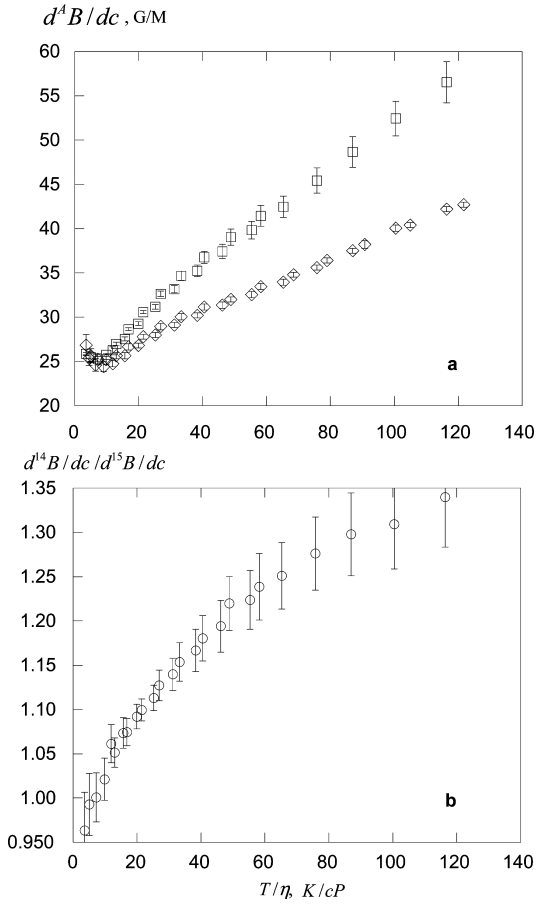

Figure 2. (a) Broadening constants $^{15}B' = d^{15}B/dc$, ◇, and $^{14}B' = d^{14}B/dc$ in 70%AG, □, taken from ref 9. (b) $^{14}B'/^{15}B' = (d^{15}B/dc)/(d^{15}B/dc)$.

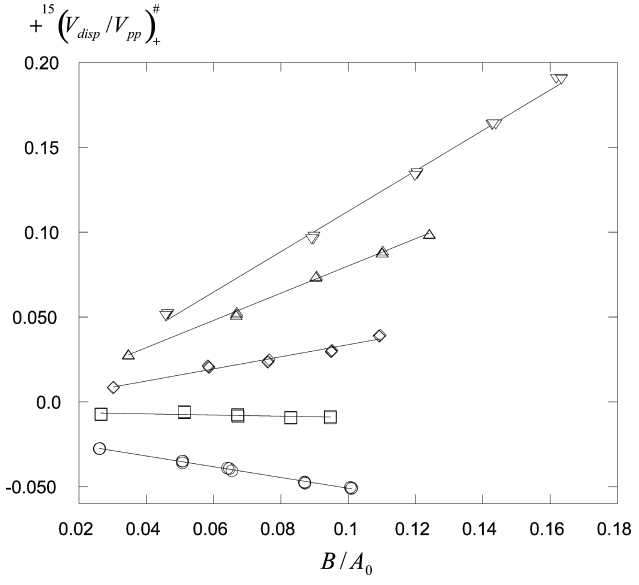

Figure 3. Normalized dispersion vs normalized broadening at 273 K, ◯; 293 K, □; 308 K, ◇; 327 K, △; and 352 K, ▽. Individual results from three spectra are shown to indicate the reproducibility. The straight lines are FITS to eq 19, yielding the slopes ^{15}k from the low-field lines. Plots of $-^{15}(V_{disp}/V_{pp})_-$ from the high-field lines are similar, yielding slopes that are averaged with the results from the low-field lines.

standard way.[15] Similarly, values of $^{15}B'_{DD}$ and $^{14}B'_{DD}$ were computed from eqs 34a and 34b. For the RBCM, values of $^{14}B'_{HSE}$ and $^{15}B'_{DD}$ were computed from eqs 33c and 34c, respectively, and the uncertainties from eqs 35 and 36.

Figure 4 shows values of $^{15}\Omega$ evaluated for the three methods. $^{15}\Omega(^{15}k)$, $^{14}\Omega(^{14}k)$, and $^{14}\Omega$(RCBM) were computed from eqs 31 and $^{15}\Omega(^{14}k)$, then $^{15}\Omega$(RCBM) were calculated using the identity eq 32a. The three methods are in agreement for $T/\eta > 80$ K/cP, below which the results from ^{14}k are larger than from ^{15}k. Results from the RBCM are in agreement with those from ^{15}k except in the region 20 K/cP < T/η < 30 K/cP. Results from the RBCM are smaller than those from ^{14}k in the region 15 K/cP < T/η < 60 K/cP.

To illustrate the effect of the diffusion model, Figure 5 shows the results for $^{15}\Omega$(RCBM) in both diffusion limits, that is, the HVL and the opposite extreme, the LVL. The upper solid line through the data is a FIT to a rational fraction to guide the eye and the lower solid line is the same FIT through the points

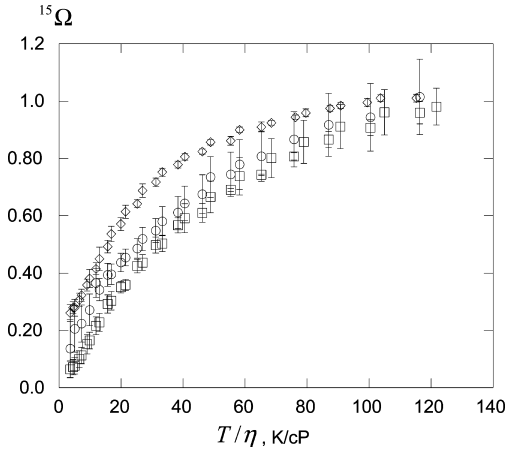

Figure 4. Values of $^{15}\Omega$ computed using the HVL from ^{14}k, ◇; ^{15}k, □; or the RBCM, ◯.

computed with the LVL. Within the precision of this experiment, the difference is negligible.

The separation of HSE and DD is given in Figures 6 and 7. In Figure 6, the left-hand ordinate is given as $^{14}B'_{HSE}$ or $(4/3)^{15}B'_{HSE}$ because these correspond to the same value of K_{ex}/γ (eq 9), which is given by the right-hand ordinate. In Figure 7, the ordinate is given as either $^{14}B'_{DD}$ or $(19/21)^{15}B'_{DD}$ because these quantities are expected to be equal according to Table 2.

Figure 6 shows that values of K_{ex} are similar using ^{15}k, ^{14}k, or the RBCM. Nevertheless, there are discrepancies that lie outside of our estimates of the random experimental uncertainties. The results using ^{15}k and RCBM are in agreement down to 30 K/cP; below that, ^{15}k predicts lower values of K_{ex}. The results using ^{14}k and RCBM are in agreement down to 50 K/cP; below that, ^{14}k predicts higher values of K_{ex} to 50 K/cP, below which the two methods are again in agreement. The straight line in Figure 6 is the SE prediction, eq 30, showing that HSE of 15pDT, and even 14pDT, in 70%AG is predicted remarkably well by simple hydrodynamic arguments. Nevertheless, some of this agreement is likely to be fortuitous as discussed in ref 8.

The data in Figure 6 were evaluated using the HVL. Using the LVL limit lowers all of the values slightly; however, the difference is within the uncertainties down to 30 G/M. Below that, the difference reaches a maximum of -2.0 ± 0.5 G/M at 273 K, the lowest point in Figure 4.

dx.doi.org/10.1021/jp505346g | J. Phys. Chem. A 2014, 118, 6154−6162

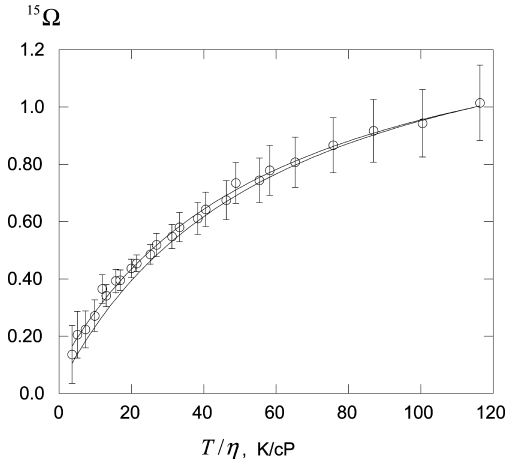

Figure 5. Effect of using the LVL, lower line, versus the HVL, upper line in the computation of $^{15}\Omega$(RCBM).

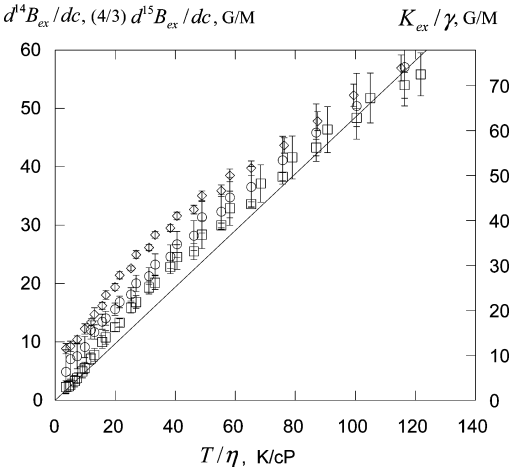

Figure 6. (a) Left-hand ordinate: values $^{14}B'_{HSE}$ determined from the ratio of the broadening constants, ◯; from ^{14}k, △;[9] and $(4/3)^{15}B'_{HSE}$ determined from ^{15}k, □. These quantities ought to give the same values of K_{ex}/γ which are given by the right-hand ordinate. The solid line is the SE prediction, eq 30.

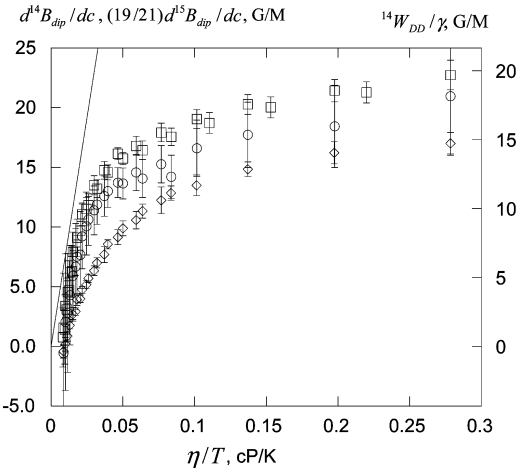

Figure 7. DD broadening constants $^{14}B'_{DD}$ and $19^{15}B'_{DD}/21$, which ought to give the same values of $^{14}W_{DD}/\gamma$, which are given by the right ordinate. Symbols the same as in Figure 6. The solid line is the SE prediction, eq 29.

Values of $^{14}B'_{DD}$ and $19^{15}B'_{DD}/21$ are displayed in Figure 7 as functions of η/T. The straight line shows the SE prediction, eq 29. Although there is general agreement between the experimental results and the hydrodynamic prediction at low values of η/T (high T), the experimental results quickly saturate to approximately 20 G/M, less than one-half of the rigid limit of 49 G/M.[14]

DISCUSSION

Is Salikhov's Theory Correct? The theory predicts that the data in Figures 4, 6, and 7 should form common curves. The curves are similar but not within our estimated random uncertainties. While the results from the RCBM are marginally different than the other two methods, partly due to rather large error bars, the results from the dispersion due to ^{14}N and ^{15}N, respectively, are clearly different from one other. At low values of T/η, the difference could be due to systematic errors due to (a) nonlinear plots of $\pm\,^{14}(V_{disp}/V_{pp})^{\#}_{\pm}$ versus $^{14}B/^{14}A_0$ for 14pDT (Figure 6 of Part 6[9]), (b) the fact that the dispersion components do not extrapolate to the origin, or (c) the interference of ^{13}C lines. Problem (a) does not apply to data in the range 20 K/cP < T/η < 50 K/cP, where, in fact, the discrepancy is particularly pronounced. Problems (b) and (c) are very unlikely to explain the discrepancy at any temperature because the lines are so similarly shaped; errors from one isotope are likely to be similar to those in the other. Note that uncertainties in the relative concentrations of the two isotopes have no effect on the values of ^{15}k or ^{14}k, and uncertainties in the temperature have a minor effect because ^{15}k and ^{14}k are slowly changing functions of the temperature.

We conclude that the theory is correct in its broad predictions; however, we cannot establish the validity of eqs 5 and 6. Perhaps better experiments could establish the details. We note that an experiment with a radical that would suppress HSE and is not hampered by ^{13}C lines could be definitive. Fremy's salt could fulfill both of these requisites provided a system can be found that is sufficiently viscous in which the radical is soluble and reasonably stable.

Relative Merits of the Dispersion vs RBCM. The dispersion method requires only one experiment and is insensitive to systematic errors in the concentration and temperature; however, fitting is necessary. The RBCM depends on simple measurements but requires two experiments where the relative concentrations and temperature are carefully controlled. Thus, the suggested experiment with Fremy's salt would require great care with a radical that is rather unstable.[1]

Relative Merits of ^{15}N and ^{14}N Nitroxides. Unless one needs the central part of the spectrum to be free for other resonance lines, ^{14}N offers several advantages, not to mention the cost. First, one has the central line that can be used to correct instrument dispersion. Second, to get to the same value of B_{HSE}/A_0, concentrations smaller by a factor of $(4/3)(^{15}A_0/^{14}A_0)$ = 1.87 are needed. Third, one has three lines instead of two from which to compute the standard deviation of the broadening. Fourth, two estimates of the rotational correlation time, τ_R, are available instead of just one.[17] The ^{15}N nitroxide does offer an increased line height by a factor of 3/2, but signal-to-noise is rarely an issue in these experiments because high concentrations are employed.

Estimating the Bimolecular Collision Rate in a Real Problem. Many studies do not have the luxury of the symmetrical spectra with small B_{inhom} that we have analyzed in this series. Complications can include overlapping spectra due to the radical being in different microenvironments or spectra at

dx.doi.org/10.1021/jp505346g | J. Phys. Chem. A 2014, 118, 6154−6162

long rotational correlation times. Extracting accurate values of V_{disp}/V_{pp} in such spectra will not prove to be easy because one needs a near-perfect fit to be confident of the results. Anyone who has tried to fit spectra with $\tau_R \geq 1$ ns knows that many parameters are involved and that FITS deemed *good* show residuals much larger than those that we have dealt with.

Thus, in some experiments, the only reliable measurement is of the line width; therefore, the RBCM is the only viable alternative. Provided that the line width varies linearly with concentration for both ^{14}N and ^{15}N, then the methods developed here will be reliable.

If it is not feasible to carry out two experiments with the two isotopes; for example, if limited sample volumes are available, then there may still be a way to proceed because values of $^{14}B'_{DD}$ reach a plateau at relatively low values of τ_R. From Figure 7 of this work, Figure 10 of Part 6, and Figure 11 of Part 8, we observe that the plateau is reached when $\tau_R > 0.2$ ns. One can usually obtain an estimate of τ_R, and in those cases in which it is larger than 0.2 ns (probably most cases), then a plateau value provides a reasonable estimate of $^{14}B'_{DD}$. We offer a tentative plateau value of $^{14}B'_{DD} = 30 \pm 12$ G/M, which is the average of the theoretical limit of 49 G/M,[14] and the experimental results in Figure 7 of this work, in Figure 10 of Part 6, and in Figure 11 of Part 8.[14] Therefore, if the broadening varies linearly with the concentration with a slope of $^{14}B'$, estimate $^{14}B'_{HSE} = {}^{14}B' - 30 \pm 12$ G/M, and compute K_{ex} from eq 9a. For most uncharged nitroxides with significant spin density on the whole molecule, the bimolecular collision rate constant is twice K_{ex}.[18] If the nitroxide is charged[19] or the spin density is delocalized,[18] then preliminary experiments in a low viscosity liquid may be necessary to find the relationship between K_{ex} and the bimolecular collision rate constant. This procedure involves errors because B_{inhom} is not taken into account; however, using perdeuterated nitroxides can reduce this error.

CONCLUSIONS

Exploiting the fact that the relative broadening constants for ^{14}N and ^{15}N nitroxides vary from $^{14}B'/{}^{15}B' = 19/21$ for DD to 4/3 for HSE, we may separate the effects of the two interactions. The factor 19/21 is valid for the HVL; in the other extreme of LVL, this factor is 14/15, 3% higher. We may also separate the effects of the two interactions in the ^{14}N experiment and also in the ^{15}N experiment by measuring the intensity of the dispersion component induced by DD and HSE. Therefore, $^{14}B'_{HSE}$ and $^{14}B'_{DD}$ may be separated as well as $^{15}B'_{HSE}$ and $^{15}B'_{DD}$ at each temperature. Because the separation in one isotope is identically related to the other, we obtain three independent measures of the separation that may be compared for consistency. In 70%AG, the three measures behave similarly with temperature; however, somewhat outside our estimates of the uncertainties due to random errors, especially when comparing the results derived from the dispersion components of 14pDT versus those from 15pDT. We conclude that Salikhov's theory[11] is correct, at least in its broad predictions.

ASSOCIATED CONTENT

Supporting Information

Correcting the intensity of the dispersion component. Microwave bridge imbalance. Correcting for a small nonlinearity between normalized broadening and normalized dispersion. Separating HSE and DD using line shifts. Explicit expressions in the LVL. This material is available free of charge via the Internet at http://pubs.acs.org.

AUTHOR INFORMATION

Notes

The authors declare no competing financial interest.

ACKNOWLEDGMENTS

M.P. gratefully acknowledges support from NIH grant 1 SC GM099635-02. Helpful discussions with Dr. K. M. Salikhov are gratefully acknowledged.

REFERENCES

(1) Bales, B. L.; Peric, M. EPR Line Shifts and Line Shape Changes Due to Spin Exchange of Nitroxide Free Radicals in Liquids. *J. Phys. Chem. B* **1997**, *101*, 8707−8716.
(2) Bales, B. L.; Peric, M. EPR Line Shifts and Line Shape Changes Due to Spin Exchange of Nitroxide Free Radicals in Liquids 2. Extension to High Spin Exchange Frequencies and Inhomogeneously Broadened Spectra. *J. Phys. Chem. A* **2002**, *106*, 4846−4854.
(3) Bales, B. L.; Peric, M.; Dragutan, I. EPR Line Shifts and Line Shape Changes Due to Spin Exchange of Nitroxide Free Radicals in Liquids 3. Extension to Five Hyperfine Lines. Additional Line Shifts Due to Re-encounters. *J. Phys. Chem. A* **2003**, *107*, 9086−9098.
(4) Bales, B. L.; Meyer, M.; Smith, S.; Peric, M. EPR Line Shifts and Line Shape Changes Due to Spin Exchange of Nitroxide-Free Radicals in Liquids 4. Test of a Method to Measure Re-encounter Rates in Liquids Employing ^{15}N and ^{14}N Nitroxide Spin Probes. *J. Phys. Chem. A* **2008**, *112*, 2177−2181.
(5) Molin, Y. N.; Salikhov, K. M.; Zamaraev, K. I. *Spin Exchange: Principles and Applications in Chemistry and Biology*; Springer-Verlag: New York, 1980; Vol. *8*, p 242.
(6) Bales, B. L.; Peric, M.; Lamy-Freund, M. T. Gaussian line broadening induced by unresolved proton hyperfine structure and by field modulation into the EPR spectrum of the proxyl spin probe. *J. Magn. Reson.* **1998**, *132*, 279−286.
(7) Salikhov, K. M. The Contribution from Exchange Interaction to Line Shifts in ESR Spectra of Paramagnetic Particles in Solutions. *J. Magn. Reson.* **1985**, *63*, 271−279.
(8) Kurban, M. R.; Peric, M.; Bales, B. L. Nitroxide spin exchange due to re-encounter collisions in a series of *n*-alkanes. *J. Chem. Phys.* **2008**, *129*, 064501−1 - 064501−10.
(9) Bales, B. L.; Meyer, M.; Smith, S.; Peric, M. EPR Line Shifts and Line Shape Changes Due to Spin Exchange of Nitroxide-Free Radicals in Liquids 6. Separating Line Broadening Due to Spin Exchange and Dipolar Interactions. *J. Phys. Chem. A* **2009**, *113*, 4930−4940.
(10) Galeev, R. T.; Salikhov, K. M. *Chem. Phys. Rep.* **1996**, *15*, 359.
(11) Salikhov, K. M. Contributions of Exchange and Dipole−Dipole Interactions to the Shape of EPR Spectra of Free Radicals in Diluted Sollutions. *Appl. Magn. Reson.* **2010**, *38*, 237−256.
(12) Peric, M.; Bales, B. L.; Peric, M. Electron Paramagnetic Line Shifts and Line Shape Changes Due to Heisenberg Spin Exchange and Dipole−Dipole Interactions of Nitroxide Free Radicals in Liquids 8. Further Experimental and Theoretical Efforts to Separate the Effects of the Two Interactions. *J. Phys. Chem. A* **2012**, *116*, 2855−2866.
(13) Abragam, A. *Principles of Nuclear Magnetism*; Oxford University Press: London, 1986.
(14) Berner, B.; Kivelson, D. The Electron Spin Resonance Line Width Method for Measuring Diffusion. A Critique. *J. Phys. Chem.* **1979**, *83*, 1406.
(15) Bevington, P. R. *Data Reduction and Error Analysis for the Physical Sciences*; McGraw-Hill: New York, 1969.
(16) Peric, I.; Merunka, D.; Bales, B. L.; Peric, M. Hydrodynamic and Non-Hydrodynamic Behavior of a Nitroxide Spin Probe in Supercooled Bulk Water. *J. Phys. Chem. B* **2014**, *118*, 7128−7135.
(17) Marsh, D., Experimental Methods in Spin-Label Spectral Analysis. In *Spin Labeling: Theory and Applications*; Plenum Publishing Corporation: New York, 1989; Vol. *8*, pp 255−303.
(18) Vandenberg, A. D.; Bales, B. L.; Salikhov, K. M.; Peric, M. Bimolecular Encounters and Re-Encounters (Cage Effect) of a Spin-Labeled Analogue of Cholestane in a Series of *n*-Alkanes: Effect of

Anisotropic Exchange Integral. *J. Phys. Chem. A* **2012**, *116*, 12460−12469.
(19) Bales, B. L.; Cadman, K. M.; Peric, M.; Schwartz, R. N.; Peric, M. Experimental Method to Measure the Effect of Charge on Bimolecular Collision Rates in Electrolyte Solutions. *J. Phys. Chem. A* **2011**, *115*, 10903−10910.